AGU PUBLICATIONS

Geophysical Research Letters

RESEARCH LETTER
10.1002/2015GL063623

Key Points:
- Dayside ULF response to pulse consistent with magnetopause surface eigenmode
- Magnetopause surface eigenmodes are a potential source of ULF waves below 2 mHz
- Magnetopause surface eigenmodes seed tailward propagating surface wave growth

Supporting Information:
- Movie S1
- Movie S2
- Movies S1 and S2

Correspondence to:
M. D. Hartinger,
mdhartin@vt.edu

Citation:
Hartinger, M. D., F. Plaschke, M. O. Archer, D. T. Welling, M. B. Moldwin, and A. Ridley (2015), The global structure and time evolution of dayside magnetopause surface eigenmodes, *Geophys. Res. Lett.*, *42*, 2594–2602, doi:10.1002/2015GL063623.

Received 24 FEB 2015
Accepted 23 MAR 2015
Accepted article online 28 MAR 2015
Published online 24 APR 2015

The global structure and time evolution of dayside magnetopause surface eigenmodes

M. D. Hartinger[1,2,3], F. Plaschke[4], M. O. Archer[5,6], D. T. Welling[2], M. B. Moldwin[2], and A. Ridley[2]

[1]Bradley Department of Electrical and Computer Engineering, Virginia Polytechnic Institute and State University, Blacksburg, Virginia, USA, [2]Department of Atmospheric, Oceanic, and Space Sciences, University of Michigan, Ann Arbor, Michigan, USA, [3]National Institute of Aerospace, Hampton, Virginia, USA, [4]Space Research Institute, Austrian Academy of Sciences, Graz, Austria, [5]Space and Atmospheric Physics, Blackett Laboratory, Imperial College London, London, UK, [6]School of Physics and Astronomy, Queen Mary University of London, London, UK

Abstract Theoretical work and recent observations suggest that the dayside magnetopause may support its own eigenmode, consisting of propagating surface waves which reflect at the northern and southern ionospheres. These magnetopause surface eigenmodes (MSEs) are a potential source of magnetospheric ultralow-frequency (ULF) waves with frequencies less than 2 mHz. Here we use the Space Weather Modeling Framework to study the magnetospheric response to impulsive solar wind dynamic pressure increases. Waves with 1.8 mHz frequency are excited whose global properties are largely consistent with theoretical predictions for MSE and cannot be explained by other known ULF wave modes. These simulation results lead to two key findings: (1) MSE can be sustained in realistic magnetic field geometries with nonzero flow shear and finite current layer thickness at the magnetopause and (2) MSE can seed the growth of tailward propagating surface waves via the Kelvin-Helmholtz instability.

1. Introduction

Ultralow-frequency (ULF) waves with discrete frequencies ≤2 mHz are often observed in the Earth's magnetosphere, both at ground-based observatories and geostationary orbit [e.g., *Samson et al.*, 1992; *Viall et al.*, 2009]. Waves with such frequencies are important for radiation belt interactions, as they can affect the relativistic electron population [e.g., *Elkington et al.*, 2003]. One mechanism proposed to explain these waves is the trapping of magnetohydrodynamic (MHD) fast wave mode energy, leading to cavity/waveguide modes with discrete frequencies set by the transit time between different boundaries in the magnetosphere [*Samson et al.*, 1992]. As discussed by *Harrold and Samson* [1992], in some regions this mechanism may require large mass densities or a cavity extending to the magnetosheath/bow shock to generate frequencies ≤2 mHz; for example, *Samson et al.* [1995] estimated typical dayside waveguide mode frequencies to be roughly 10 mHz. Another mechanism, direct driving by solar wind density fluctuations, often, though not always, generates waves with frequencies ≤2 mHz in the dayside magnetosphere. In particular, *Viall et al.* [2009]—using simultaneous observations in the dayside magnetosphere and solar wind—found that "discrete magnetospheric oscillations in the $f = 0.5–5.0$ mHz range are directly driven by periodic solar wind number density structures 54% of the time that the solar wind contains periodic number density structures."

Anderson et al. [1968] first presented observational evidence of periodic magnetopause motion with frequencies below 2 mHz. Motivated by these observations, *Smit* [1968] treated subsolar magnetopause motion as a damped simple harmonic oscillator, finding natural frequencies in the range of a few mHz. Later models found similar response frequencies [*Freeman et al.*, 1995; *Børve et al.*, 2011]. *Plaschke et al.* [2009a] showed that dayside magnetopause oscillation periods tend to have frequencies of a few mHz and recur at specific frequencies. They further compared these magnetopause oscillations with previously observed quasi-steady magnetospheric ULF wave activity of similar frequency, suggesting a mechanism for ULF wave generation related to natural magnetopause frequencies. *Plaschke and Glassmeier* [2011] examined how the dayside magnetopause could support an eigenmode; in particular, propagating surface waves reflect at the northern and southern ionospheres and form a standing wave. Unlike the models of *Smit* [1968], *Freeman et al.* [1995], and *Børve et al.* [2011], their model explicitly treats surface wave propagation at the dayside magnetopause and trapping by the ionosphere, leading to frequencies comparable to or lower than the other models.

Plaschke and Glassmeier [2011] modeled surface wave trapping by using ideal, single-fluid, incompressible MHD and a two-slab geometry, treating the magnetosphere as a box with reflecting ionospheric boundary conditions and the magnetosheath as an open slab without such boundary conditions. The magnetopause is taken to be an infinitely thin current sheet, and there is no bulk flow along the boundary. With these conditions, the magnetopause supports two coupled, evanescent magnetosonic waves—one on either side of the magnetopause—leading to a magnetopause surface eigenmode (MSE). Citing early work by *Kruskal and Schwarzschild* [1954] demonstrating the propagation of surface waves at interfaces between different plasma regimes, *Plaschke and Glassmeier* [2011] also referred to these waves as Kruskal-Schwarzschild modes. Some key properties of MSE from *Plaschke and Glassmeier* [2011] are as follows:

1. Magnetopause motion associated with the MSE generates compressional magnetic perturbations that are 180° out of phase on either side of the magnetopause boundary (as the magnetosphere is compressed, the magnetosheath is rarefied, and vice versa). For the fundamental MSE, the largest perturbations ought to be near the equatorial plane.
2. For the fundamental MSE, transverse magnetic perturbations ought to be largest near the ionosphere and exhibit a 180° phase difference on either side of the magnetic equator [*Plaschke and Glassmeier*, 2011, equation (35)].
3. All perturbations associated with MSE decay with distance from the magnetopause.
4. MSE frequencies are in the range of a few mHz, based on calculations by *Plaschke and Glassmeier* [2011] and *Archer et al.* [2013b]. These frequencies are related to the transit time of the surface waves between the different boundaries rather than an external driving frequency. As such, MSE provide a possible mechanism to explain monochromatic ULF responses to drivers with a broadband frequency spectrum.
5. MSE do not require a Kelvin-Helmholtz (KH) unstable magnetopause to grow.

Recent observational studies suggest that MSEs generate monochromatic ULF waves in the magnetosphere. *Plaschke et al.* [2009b] found that dayside magnetopause oscillations occur preferentially during solar wind conditions favorable for generating MSE, suggesting an MSE generation mechanism. *Hietala et al.* [2012] observed high-speed magnetosheath jets that resulted in localized magnetopause displacements and ULF perturbations at geostationary orbit; *Plaschke et al.* [2013] further linked these jets and resultant ULF oscillations to MSE, discussing how localized impulses on the magnetopause drive the required MSE current system. *Archer et al.* [2013a, 2013b] used simultaneous observations in the magnetosheath and magnetosphere at geostationary orbit to show that high-speed magnetosheath jets impacting the magnetopause drive ULF waves in the magnetosphere with discrete frequencies consistent with MSE.

Despite this evidence, it is not clear whether MSEs play an important role in driving magnetospheric ULF waves. To date, no modeling studies examining dayside magnetopause oscillations have simultaneously taken into account the geometry of the Earth's three-dimensional distorted dipolar magnetic field, finite thickness of the magnetopause boundary layer/current sheet, finite flow in the magnetosheath, and reflective ionospheric boundary conditions; all of these factors affect MSE, and some, such as finite magnetosheath flow and boundary layer thickness, may reduce their occurrence [*Plaschke and Glassmeier*, 2011]. Moreover, it is difficult to observationally test the predictions of *Plaschke and Glassmeier* [2011] for MSE due to their large length scales and long periods, as well as the presence of other ULF wave activity near the magnetopause. The goal of this letter is to extend previous observational and theoretical work by examining MSE properties in a global, three-dimensional MHD simulation coupled to an ionosphere model. We aim to test whether MSEs occur in realistic magnetic field geometries with finite flow shear and current sheet thickness and to determine how these factors affect MSE properties.

2. MHD Simulation Description

We use the Space Weather Modeling Framework (SWMF) for simulating MSE. SWMF couples several models used for different physics domains [*Tóth et al.*, 2005]. We use two SWMF models for this simulation: a single-fluid version of the Block Adaptive Tree Solar-wind Roe-type Upwind Scheme (BATS-R-US) [*Powell et al.*, 1999] for the magnetosphere coupled to the Ridley Ionosphere Model (RIM) [*Ridley and Liemohn*, 2002; *Ridley et al.*, 2004]. BATS-R-US and RIM are coupled by combining field-aligned currents mapped from the inner boundary of BATS-R-US, the $F_{10.7}$ flux (a constant in these simulations), and an empirical model to obtain conductances. Using a Poisson-type equation, electric potentials are obtained on the RIM grid, and these are mapped back to the inner boundary of BATS-R-US.

This SWMF configuration is similar to the setup used by *Hartinger et al.* [2014] to study the effect of magnetopause motion on MHD fast-mode waves in the Earth's magnetosphere. The Earth's dipole axis is set parallel to the rotation axis, and we use a simulation domain of x from −96 to 32 R_E, y from −64 to 64 R_E, and z from −64 to 64 R_E (x, y, and z are equivalent to SM coordinates here), where the inner boundary of BATS-R-US is a sphere at $r = 2.5$ R_E. BATS-R-US uses a Cartesian grid with variable grid cell size. The grid cells have widths of 1/8 R_E in the region from $-16 \leq x \leq 32$, $-16 \leq y \leq 16$, and $-16 \leq z \leq 16$, with gradually decreasing cell dimensions outside of this region. However, to better resolve current systems with small perpendicular scales near the inner boundary of BATS-R-US, we also added a spherical shell of higher-resolution 1/16 R_E grid cells between 2.5 (inner boundary) and 4.5 R_E. We examined the effect of numerical dissipation on our simulation results, and this will be discussed further in section 4. Finally, dayside ionospheric conductivities near the open-closed field line boundary in RIM are roughly 5 mhos.

We use idealized solar wind driving conditions to examine the structure of MSE while avoiding complications associated with the presence of other phenomena, such as dayside reconnection; future work will include more realistic driving conditions. In this simulation, the solar wind magnetic field is northward ($\mathbf{B} = (0, 0, 5)$ nT) and the solar wind speed is 450 km/s ($\mathbf{V} = (-450, 0, 0)$ km/s). The background solar wind density, n_0, is 6.0 amu per cm^3, but we introduce density (dynamic pressure) pulses with normal vectors in the x direction to potentially excite MSE. When examining wave properties, we use field-aligned (FA) coordinates where z is along the background magnetic field, y points approximately eastward (orthogonal to z in the plane defined by z and the eastward pointing unit vector), and x completes the right-handed orthogonal set pointing radially outward at the magnetic equator. The background magnetic field that defines z is the unperturbed value obtained just before the arrival of the density pulse (instantaneous value at 200 min from the beginning of the simulation). All perturbed quantities are obtained by subtracting the initial value before the pulse, at 200 min simulation time.

3. MHD Simulation Results

Figure 1 (top) shows the solar wind density at position $\mathbf{r} = [20, 0, 0]$ R_E, with density doubling to 12 amu/cm^3 before returning to the background value of 6 amu/cm^3 over a period of roughly 3 min. Though the pulse is affected by numerical dissipation, its properties—e.g., its duration—do not change substantially between this position and the magnetopause. The 3 min time scale corresponds to a length scale in the solar wind of roughly 13 R_E; this time scale is roughly 3 times smaller than both the typical dayside quasi-static response period [e.g., *Børve et al.*, 2011] and the fundamental MSE period. We shall make no statement in this study about the effectiveness of different solar wind length (and time) scales in exciting MSE; this is an important topic for future work, but the first step and focus of this study is to establish whether a realistic dayside magnetopause geometry with finite flow shear and current layer thickness can support MSE.

In the aftermath of the pressure pulse, a ULF response is seen in the field-aligned magnetic field perturbation at $\mathbf{r} = [9, 0, 0]$ R_E, as shown in the second panel as a solid blue line; note that the equilibrium subsolar magnetopause is located at 10.2 R_E and is not displaced inward as far as 9 R_E during the period of interest. The second panel also shows the electric field y perturbation as a solid red line, which is 140° out of phase with the magnetic field (average phase difference over the duration of the event, based on cross-phase analysis).

To examine the field-aligned structure of these waves, we select points near the ionosphere/open-closed field line boundary that are magnetically conjugate to our original observation point at $\mathbf{r} = [9, 0, 0]$ R_E. The second panel of Figure 1 (top) shows the magnetic field z perturbation at $\mathbf{r} = [2, 0, 4]$ R_E (blue dashed line) and $\mathbf{r} = [2, 0, -4]$ R_E (blue crosses). The perturbation amplitude is much smaller near the inner boundary/ionosphere. The third panel of Figure 1 (top) shows the magnetic field x perturbation at $\mathbf{r} = [9, 0, 0]$ R_E (solid black line), $\mathbf{r} = [2, 0, 4]$ R_E (black dashed line), and $\mathbf{r} = [2, 0, -4]$ R_E (black crosses). Unlike the z component, the x component has the smallest amplitude near the equator and largest amplitude near the ionosphere. Moreover, there is a 180° phase difference between the north and south ionosphere perturbations. The fourth panel of Figure 1 (top) shows the same information but for the magnetic field y perturbation. It exhibits the same trends as the x component: negligible amplitude near the equator, large amplitude near the ionosphere, and 180° phase difference between the north and south hemisphere. Comparing the solid blue line in the second panel and solid black lines in the third and fourth panels, it is clear that the wave activity is strongly compressional near the equatorial plane.

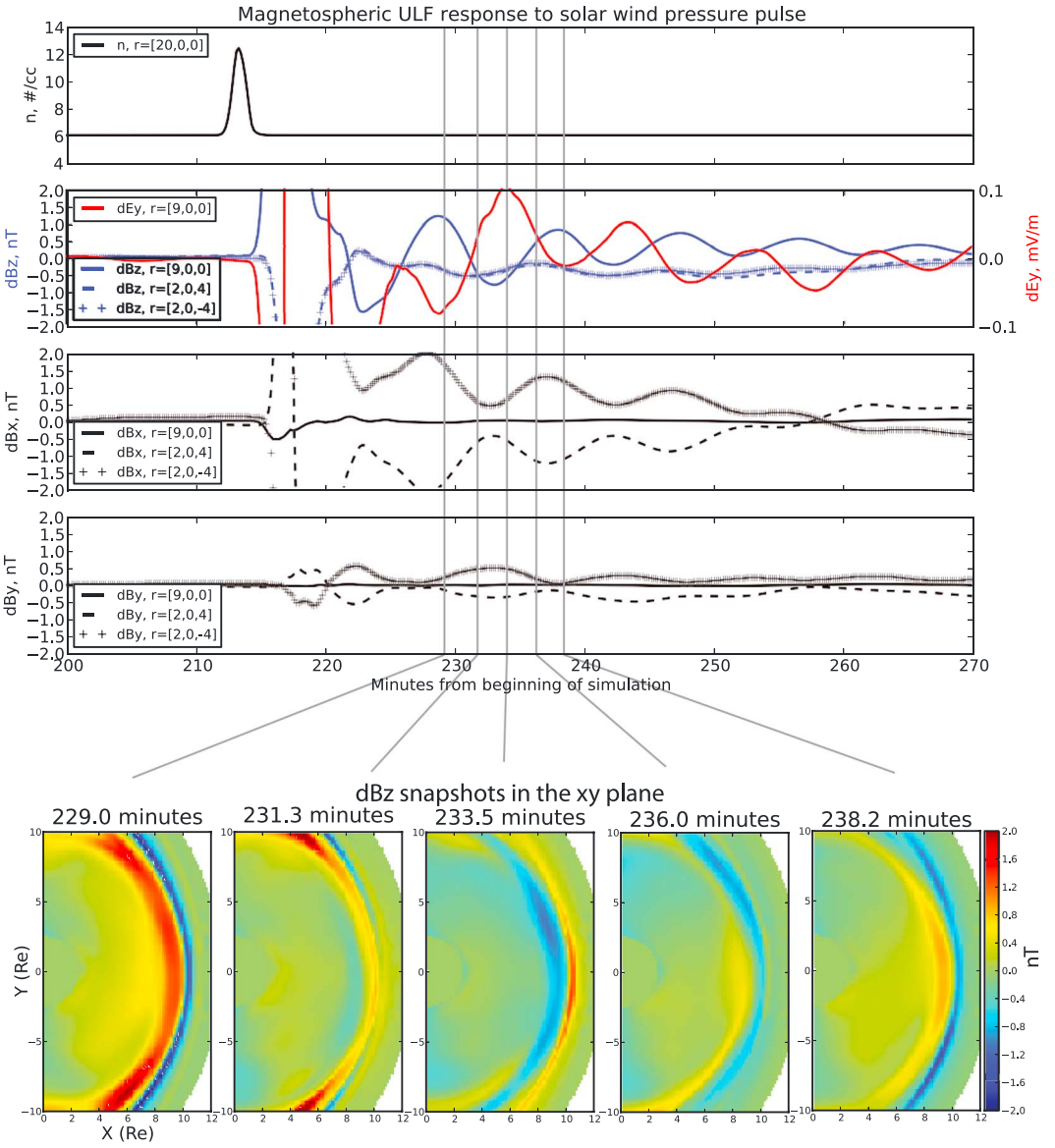

Figure 1. (top) The top four panels show the solar wind density (first panel); magnetic (solid blue, *z* component) and electric (red, *y* component) perturbation fields at $r = [9, 0, 0]$ as well as magnetic field *z* perturbations at $r = [2, 0, 4]$ (dashed blue) and $r = [2, 0, -4]$ (crosses) (second panel); the magnetic field *x* perturbation at $r = [9, 0, 0]$ (solid black), $r = [2, 0, 4]$ (dashed black), and $r = [2, 0, -4]$ (black crosses) (third panel); and the same as the third panel but for the magnetic field *y* perturbation (fourth panel). (bottom) Snapshots of the *z* component of the perturbation magnetic field are shown for the *xy* (SM coordinates) plane at different times corresponding to the gray lines in the top part of the figure.

More information about the spatial structure of the magnetic field *z* perturbation is shown in Figure 1 (bottom). In all figures, data are masked where the background magnetic field magnitude is less than 20 nT to remove low magnetic field regions where the FA coordinate transformation is less reliable. Snapshots of the magnetic field *z* perturbation are shown for the *xy* plane (SM coordinates) at different times corresponding to the gray lines in the top part of the figure. As shown at the left (*xy* plane at 229 min), the magnetic field is initially compressed (elevated above background, indicated by the color red) inside the magnetopause and rarefied outside the magnetopause (indicated by the color blue). At 233.5 min, the situation is reversed, with rarefied fields inside the magnetopause and compressed fields outside. Finally, the magnetosphere returns to the initial configuration (compressed inside, rarefied outside) at 238.2 min. These features are consistent with a small inward and outward displacement of the magnetopause (roughly 0.2 R_E displacement at the subsolar point—equivalent to one to two grid cells), as is the fact that the largest perturbations

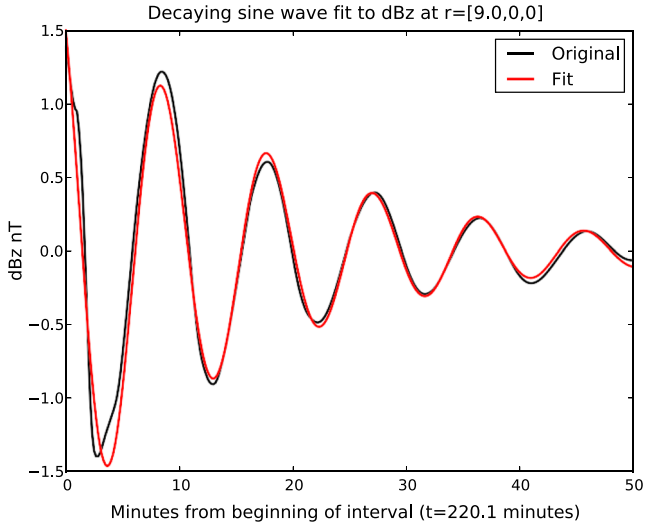

Figure 2. This figure shows the magnetic field z perturbation at $r = [9, 0, 0]$ as a black line; the data are the same as in Figure 1 except that a second-order polynomial is fit to the data and subtracted to remove a small, slowly varying trend. The red line shows a least squares fit to a function of the form $A_0 e^{-\frac{t}{\tau}} \sin(\omega t + \phi)$.

(indicated by dark red and blue colors) are confined to the region near the magnetopause and decay with increasing distance from the boundary.

The response in the z component of the magnetic field appears nearly monochromatic and decays over many wave cycles (e.g., second panel of Figure 1, top). To extract the wave frequency and damping constant, we subtract a second-order polynomial fit to the data (to remove a small, slowly varying trend) then fit a function of the form $A_0 e^{-\frac{t}{\tau}} \sin(\omega t + \phi)$ to these data for the period between 220 and 270 min. The result of the least squares fit is shown in Figure 2 as a red line, with a black line indicating the original time series. The initial amplitude at 220 min, A_0, is 1.80 nT, and the phase ϕ is 2.15 radians. The fit frequency, $f(\omega/2\pi)$, is 1.79 mHz (9.31 min period). Finally, the decay constant, τ, is 1070 s. Based on the values for τ and ω, MSEs damp faster than standing Alfvén waves in the dayside magnetosphere but slower than nightside standing Alfvén waves [*Newton et al.*, 1978].

For the period between 224.17 and 266.83 min, we extract magnetic field z perturbations in the xy and xz planes every 10 s. Using a 256-point discrete Fourier transform with three-point smoothing in the frequency domain, we compute the power spectral density (PSD) at every spatial point for each of these parameters. Figure 3a shows the spatial structure of $\sqrt{\text{PSD}}$ for the magnetic field z perturbation in the xy plane for a frequency bin centered on 1.6 mHz—the bin that overlaps the MSE frequency and exhibits the peak PSD—normalized to the maximum value in the figure. Here normalized $\sqrt{\text{PSD}}$ at 1.6 mHz can be used as a proxy for the normalized, root-mean-square (RMS) ULF wave amplitude, dBz. A mask is applied inside of 2.5 R_E (inner boundary of BATS-R-US), and, as before, an additional mask is applied where $|B| < 20$ nT. The largest perturbations are localized to the magnetopause, with decreasing amplitude with increasing distance from the boundary. A dawn-dusk asymmetry exists near the subsolar point (peak dBz postnoon inside the magnetopause) due to dawn-dusk asymmetries in RIM. In particular, the RIM version used here includes a dawn-dusk asymmetry in conductance to account for asymmetries in particle precipitation/conductance near the auroral oval [*Ridley et al.*, 2004, section 5]. These conductance asymmetries alter current systems and pressure in BATS-R-US [*Ridley et al.*, 2004], including the MSE current system.

Figure 3b shows the same data but in the xz plane; the normalization factor is also the same. For reference, two magnetic field lines are shown in purple, the inner one representing the outermost dipolar field line and the outer representing the last closed field line. The largest perturbations are seen near the magnetopause and near the equatorial plane. The two field lines indicate a more complicated geometry for the dayside magnetosphere than the straight field lines in *Plaschke and Glassmeier* [2011]. Two regions of enhanced wave activity are evident just inside the dipolar field line at $\mathbf{r} = [5.5, 0, \pm 5]$ R_E. We attribute this enhanced wave activity to a high-latitude Kelvin-Helmholtz (KH) instability, similar to what was reported in the

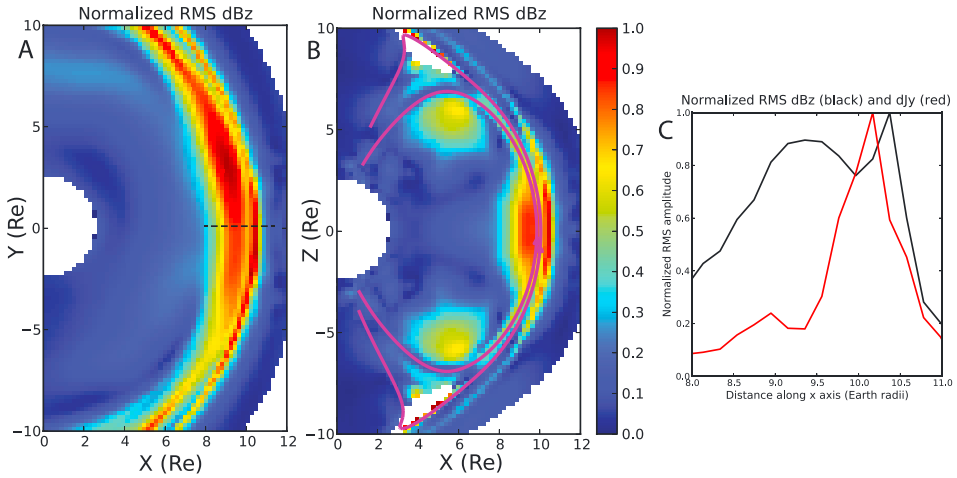

Figure 3. (a) RMS amplitude of the magnetic field *z* perturbation at the MSE frequency, normalized to the maximum value in the figure and shown in the *xy* plane. (b) The same for the magnetic field *z* perturbation in the *xz* plane; here the data are normalized to the same value is in Figure 3a. Purple lines are used for two representative magnetic field lines. (c) Normalized RMS amplitude ($\sqrt{\text{PSD}}$) for the magnetic field *z* perturbation at different points along the *x* axis (black line, same data as Figures 3a and 3b, taken from the area marked by the black dashed line in Figure 3a). The normalized RMS amplitude of the east-west current perturbation is also shown (red line), where the normalization factor is the maximum value in the *xy* plane (as was the case for the magnetic perturbation).

simulation results of *Takahashi et al.* [2012] (e.g., Figure 15 in that study). We shall discuss this feature further in section 4.

In both Figures 3a and 3b, there is a local minima in dBz at the magnetopause. The black line in Figure 3c shows the same data as in Figure 3a, except limited to a section of the *x* axis (indicated by the black dashed line in Figure 3a). The local minimum is clear at roughly 10 R_E. This corresponds to the peak in $\sqrt{\text{PSD}}$ for the *y* component of the current perturbation, as shown by the red line (data normalized to the maximum value in the *xy* plane). Since the current sheet has finite thickness, dBz has multiple peaks surrounding the region with peak current perturbation.

4. Discussion

To summarize, we conducted a global MHD simulation with steady driving conditions apart from an impulse in the solar wind density. We now compare our observations with several possible ULF wave modes and ULF wave generation mechanisms:

1. *Standing Alfvén Waves*. For standing Alfvén waves excited by a solar wind pressure pulse, in the absence of cavity modes, MSE, or some other frequency selection mechanism, one generally expects a continuum of frequencies to be excited in the magnetosphere [*Dungey*, 1967]. Additionally, for a solar wind driver symmetric with respect to noon (as in this simulation), coupling between the fast and shear Alfvén wave modes is weakest at noon and thus standing Alfvén waves driven by the solar wind should increase in amplitude as one moves away from noon [e.g., *Claudepierre et al.*, 2010]. In contrast, the waves we are interested in have largest amplitudes near noon and at a discrete frequency. Moreover, standing Alfvén waves occur on closed field lines, whereas we observe coherent ULF wave activity on either side of the open-closed field line boundary.
2. *Trapped Fast-Mode Waves (Cavity or Waveguide Mode)*. For a driver symmetric with respect to noon, one expects trapped fast MHD wave modes to appear like cavity modes near noon: radially standing fast MHD wave modes (east-west electric field 90° out of phase with the compressional magnetic field) with nodes and antinodes in the electric and magnetic field at different locations [e.g., *Waters et al.*, 2002]. In contrast, the simulated perturbations are 140° out of phase, and they decay monotonically with increasing distance from the magnetopause.
3. *Compressional Waves Directly Driven by the Solar Wind*. We can exclude this possibility as, by design, there are no waves in the solar wind and no perturbations apart from the density pulse.

4. *Quasiperiodic Dayside Reconnection*. We suppressed reconnection in this simulation by restricting to a steady, northward IMF condition. There is no evidence for periodic flux transfer events when examining the *xy* and *xz* plane animations (supporting information).
5. *Kelvin-Helmholtz Instability*. The KH instability is usually thought to be most important for driving ULF waves near the flank regions of the magnetosphere, where velocity shear is largest [*Farrugia et al.*, 1998]. In contrast, we observe the largest wave amplitudes near the subsolar/stagnation point, where the velocity shear is smallest/zero. Moreover, we know of no mechanism where a KH unstable magnetopause, by itself, could trap wave energy in the dayside magnetosphere long after an initial solar wind density pulse seeds surface wave growth (recall the pulse duration is 3 min and the waves are observed for nearly an hour following the pulse). Thus, the KH instability is not the necessary ingredient for driving the ULF wave activity in the aftermath of the pulse, though, once seeded by the MSE, it drives the growth of tailward propagating surface waves, as will be discussed further.
6. *Magnetopause Surface Eigenmode*. *Plaschke and Glassmeier* [2011] predicted several features of MSE consistent with the simulated wave activity (Figures 1–3): predominately compressional waves localized near the magnetopause and the equatorial plane, largest transverse magnetic perturbations near the ionosphere, 180° phase difference between transverse magnetic perturbations on either side of the magnetic equator, wave activity that lasts many cycles, discrete frequency pulsations excited by a broadband frequency driver, and frequencies lower than 2 mHz.

We conclude that the simulated ULF wave is an MSE. This is an important result, as to our knowledge no previous study has documented the presence or properties of MSE in a realistic magnetic field geometry and in the presence of flow shear and finite current sheet thickness at the magnetopause.

As shown in Figure 3c, the spreading of MSE current perturbations over a finite boundary layer leads to a local minimum in the compressional magnetic perturbation. This feature is not present in the model of *Plaschke and Glassmeier* [2011], since it treats the magnetopause as a discontinuity with vanishing thickness. The current perturbations in Figure 3c extend over a region of roughly 0.8 R_E (full width at half maximum); this is significantly larger than typically observed magnetopause current sheet thicknesses, which are on the order of 0.1 R_E [*Berchem and Russell*, 1982] (global MHD simulations cannot resolve current sheets with thicknesses on the order of ion gyroradii). For this reason, this local minimum would likely appear smaller in observations or other simulations.

The persistence of the MSE for many wave cycles demonstrates that damping due to wave-mode conversion at thick magnetopause boundary layers [*Chen and Hasegawa*, 1974] does not preclude the occurrence of MSE. The damping rate found in this simulation is likely an upper bound for MSE damping in the real magnetosphere, since BATS-R-US and other numerical simulations are subject to numerical dissipation. We found that MSE damping rates are reduced when increasing grid resolution near the inner boundary, since MSE current systems are better resolved. However, results are qualitatively similar between high- and low-resolution runs. It is possible that the damping rate reported in this study would decrease further if higher-resolution grids were used, but this would not change the conclusions of this study.

The thickness of the magnetopause boundary layer—as well as other factors present in the simulation but not in the model of *Plaschke and Glassmeier* [2011]—affects the surface wave dispersion relation and time-of-flight (TOF) MSE frequency estimates. We calculated the expected fundamental frequency for our simulated MSE using the dispersion relation from *Plaschke and Glassmeier* [2011] and a TOF estimate applied to the dispersion relation. We found frequencies of roughly 1.3 mHz, lower than the observed frequency of 1.8 mHz (a 28% difference). This is likely because the dispersion relation used by *Plaschke and Glassmeier* [2011] and *Archer et al.* [2013b] to estimate TOF frequencies for MSE assumes an incompressible plasma and an infinitely thin boundary layer. Relaxing either of these assumptions changes the dispersion relation and thus the wave speed and TOF frequency. We emphasize that the simulated frequency of 1.8 mHz is in the expected range for MSE frequencies and is roughly consistent with the dayside trapping of surface wave activity by the ionosphere [*Archer et al.*, 2013b].

Turning now to the effect of finite magnetosheath flows on MSE properties, these simulation results show that even for moderately elevated solar wind flow speed (450 km/s), flow shear at the magnetopause boundary layer does not prevent the occurrence of MSE. Furthermore, MSE can seed the growth of tailward propagating surface waves at both equatorial and high latitudes. For example, Figures 1 (bottom), 3a, and supporting information Movie S1 all indicate regions of enhanced wave activity away from the subso-

lar point; i.e., moving eastward or westward along the magnetopause, the magnetic field *z* perturbation amplitude first decreases with increasing distance from the subsolar point then increases again as the MSE seeds the growth of larger-amplitude waves via the KH instability. The same is true as one moves away from the subsolar point to high latitudes, as shown in Figure 3b and supporting information Movie S2. In both cases, the MSE provides seed perturbations that destabilize the magnetopause; these perturbations can then extract energy from magnetosheath flows, rapidly growing via the KH instability as they move away from the subsolar point toward regions with increasing flow shear [e.g., *Farrugia et al.*, 1998]. These results suggest that although the MSE is generated in the dayside magnetosphere, its effects may be felt elsewhere. Understanding MSE growth/propagation in the presence of a KH unstable magnetopause is an important topic for future work.

5. Summary

We used BATS-R-US global MHD simulations to study the response of the magnetosphere to a solar wind density/dynamic pressure impulse. We found persistent, monochromatic wave activity in the aftermath of the pulse with global properties largely consistent with theoretical predictions for magnetopause surface eigenmodes (MSE) yet inconsistent with other known ULF wave modes. We thus demonstrated that MSE can exist in a realistic magnetic field geometry with nonzero flow shear, finite magnetopause current sheet thickness, and reflective ionospheric boundaries, and we showed how these features change the properties of MSE when compared to idealized models without these features. There are two main implications of this work: (1) MSEs are a viable mechanism for explaining monochromatic, compressional ULF waves in the dayside magnetosphere with frequencies less than 2 mHz and (2) MSE can provide a seed perturbation for the growth of large-amplitude, tailward propagating surface waves due to the KH instability.

Acknowledgments

M.D. Hartinger was funded through NSF grant AGS-1230398. We would like to acknowledge high-performance computing support from Yellowstone (ark:/85065/d7wd3xhc) provided by NCAR's Computational and Information Systems Laboratory, sponsored by the National Science Foundation. This work was carried out using the SWMF/BATS-R-US tools developed at the University of Michigan Center for Space Environment Modeling (CSEM). Simulation output files are available upon request from the corresponding author (M.D. Hartinger, mdhartin@vt.edu). The authors thank both reviewers for their efforts in evaluating this paper.

The Editor thanks Karl-Heinz Glassmeier and an anonymous reviewer for their assistance in evaluating this paper.

References

Anderson, K. A., J. H. Binsack, and D. H. Fairfield (1968), Hydromagnetic disturbances of 3- to 15-minute period on the magnetopause and their relation to bow shock spikes, *J. Geophys. Res.*, *73*, 2371–2386, doi:10.1029/JA073i007p02371.

Archer, M. O., T. S. Horbury, J. P. Eastwood, J. M. Weygand, and T. K. Yeoman (2013a), Magnetospheric response to magnetosheath pressure pulses: A low-pass filter effect, *J. Geophys. Res. Space Physics*, *118*, 5454–5466, doi:10.1002/jgra.50519.

Archer, M. O., M. D. Hartinger, and T. S. Horbury (2013b), Magnetospheric "magic" frequencies as magnetopause surface eigenmodes, *Geophys. Res. Lett.*, *40*, 5003–5008, doi:10.1002/grl.50979.

Berchem, J., and C. T. Russell (1982), The thickness of the magnetopause current layer—ISEE 1 and 2 observations, *J. Geophys. Res.*, *87*, 2108–2114, doi:10.1029/JA087iA04p02108.

Børve, S., H. Sato, H. L. Pécseli, and J. K. Trulsen (2011), Minute-scale period oscillations of the magnetosphere, *Ann. Geophys.*, *29*, 663–671, doi:10.5194/angeo-29-663-2011.

Chen, L., and A. Hasegawa (1974), A theory of long-period magnetic pulsations: 2. Impulse excitation of surface eigenmode, *J. Geophys. Res.*, *79*, 1033–1037, doi:10.1029/JA079i007p01033.

Claudepierre, S. G., M. K. Hudson, W. Lotko, J. G. Lyon, and R. E. Denton (2010), Solar wind driving of magnetospheric ULF waves: Field line resonances driven by dynamic pressure fluctuations, *J. Geophys. Res.*, *115*, A11202, doi:10.1029/2010JA015399.

Dungey, J. W. (1967), Hydromagnetic waves, in *Physics of Geomagnetic Phenomena*, edited by S. Matsushita and W. H. Campbell, pp. 913–934, Academic Press, New York.

Elkington, S. R., M. K. Hudson, and A. A. Chan (2003), Resonant acceleration and diffusion of outer zone electrons in an asymmetric geomagnetic field, *J. Geophys. Res.*, *108*(A3), 1116, doi:10.1029/2001JA009202.

Farrugia, C. J., F. T. Gratton, L. Bender, H. K. Biernat, N. V. Erkaev, J. M. Quinn, R. B. Torbert, and V. Dennisenko (1998), Charts of joint Kelvin-Helmholtz and Rayleigh-Taylor instabilities at the dayside magnetopause for strongly northward interplanetary magnetic field, *J. Geophys. Res.*, *103*, 6703–6728, doi:10.1029/97JA03248.

Freeman, M. P., N. C. Freeman, and C. J. Farrugia (1995), A linear perturbation analysis of magnetopause motion in the Newton-Busemann limit, *Ann. Geophys.*, *13*, 907–918, doi:10.1007/s00585-995-0907-0.

Harrold, B. G., and J. C. Samson (1992), Standing ULF modes of the magnetosphere—A theory, *Geophys. Res. Lett.*, *19*, 1811–1814, doi:10.1029/92GL01802.

Hartinger, M. D., D. Welling, N. M. Viall, M. B. Moldwin, and A. Ridley (2014), The effect of magnetopause motion on fast mode resonance, *J. Geophys. Res. Space Physics*, *119*, 8212–8227, doi:10.1002/2014JA020401.

Hietala, H., N. Partamies, T. V. Laitinen, L. B. N. Clausen, G. Facskó, A. Vaivads, H. E. J. Koskinen, I. Dandouras, H. Rème, and E. A. Lucek (2012), Supermagnetosonic subsolar magnetosheath jets and their effects: From the solar wind to the ionospheric convection, *Ann. Geophys.*, *30*, 33–48, doi:10.5194/angeo-30-33-2012.

Kruskal, M., and M. Schwarzschild (1954), Some instabilities of a completely ionized plasma, *Proc. R. Soc. London, Ser. A*, *223*, 348–360, doi:10.1098/rspa.1954.0120.

Newton, R. S., D. J. Southwood, and W. J. Hughes (1978), Damping of geomagnetic pulsations by the ionosphere, *Planet. Space Sci.*, *26*, 201–209, doi:10.1016/0032-0633(78)90085-5.

Plaschke, F., and K.-H. Glassmeier (2011), Properties of standing Kruskal-Schwarzschild-modes at the magnetopause, *Ann. Geophys.*, *29*, 1793–1807, doi:10.5194/angeo-29-1793-2011.

Plaschke, F., K.-H. Glassmeier, H. U. Auster, O. D. Constantinescu, W. Magnes, V. Angelopoulos, D. G. Sibeck, and J. P. McFadden (2009a), Standing Alfvén waves at the magnetopause, *Geophys. Res. Lett.*, *36*, L02104, doi:10.1029/2008GL036411.

Plaschke, F., K.-H. Glassmeier, D. G. Sibeck, H. U. Auster, O. D. Constantinescu, V. Angelopoulos, and W. Magnes (2009b), Magnetopause surface oscillation frequencies at different solar wind conditions, *Ann. Geophys.*, *27*, 4521–4532, doi:10.5194/angeo-27-4521-2009.

Plaschke, F., H. Hietala, and V. Angelopoulos (2013), Anti-sunward high-speed jets in the subsolar magnetosheath, *Ann. Geophys.*, *31*, 1877–1889, doi:10.5194/angeo-31-1877-2013.

Powell, K. G., P. L. Roe, T. J. Linde, T. I. Gombosi, and D. L. De Zeeuw (1999), A solution-adaptive upwind scheme for ideal magnetohydrodynamics, *J. Comput. Phys.*, *154*, 284–209, doi:10.1006/jcph.1999.6299.

Ridley, A. J., and M. W. Liemohn (2002), A model-derived storm time asymmetric ring current driven electric field description, *J. Geophys. Res.*, *107*(A8), 1151, doi:10.1029/2001JA000051.

Ridley, A, T. Gombosi, and D. De Zeeuw (2004), Ionospheric control of the magnetosphere: Conductance, *Ann. Geophys.*, *22*, 567–584, doi:10.5194/angeo-22-567-2004.

Samson, J. C., B. G. Harrold, J. M. Ruohoniemi, R. A. Greenwald, and A. D. M. Walker (1992), Field line resonances associated with MHD waveguides in the magnetosphere, *Geophys. Res. Lett.*, *19*, 441–444, doi:10.1029/92GL00116.

Samson, J. C., C. L. Waters, F. W. Menk, and B. J. Fraser (1995), Fine structure in the spectra of low latitude field line resonances, *Geophys. Res. Lett.*, *22*, 2111–2114, doi:10.1029/95GL01770.

Smit, G. R. (1968), Oscillatory motion of the nose region of the magnetopause, *J. Geophys. Res.*, *73*, 4990–4993, doi:10.1029/JA073i015p04990.

Takahashi, K., K. Yumoto, S. G. Claudepierre, E. R. Sanchez, O. A Troshichev, and A. S. Janzhura (2012), Dependence of the amplitude of Pc5-band magnetic field variations on the solar wind and solar activity, *J. Geophys. Res.*, *117*, A04207, doi:10.1029/2011JA017120.

Tóth, G., et al. (2005), Space Weather Modeling Framework: A new tool for the space science community, *J. Geophys. Res.*, *110*, A12226, doi:10.1029/2005JA011126.

Viall, N. M., L. Kepko, and H. E. Spence (2009), Relative occurrence rates and connection of discrete frequency oscillations in the solar wind density and dayside magnetosphere, *J. Geophys. Res.*, *114*, A01201, doi:10.1029/2008JA013334.

Waters, C. L., K. Takahashi, D.-H. Lee, and B. J. Anderson (2002), Detection of ultralow-frequency cavity modes using spacecraft data, *J. Geophys. Res.*, *107*(A10), 1284, doi:10.1029/2001JA000224.